

**Ferroelectric to incommensurate fluctuations crossover in  $\text{PbHfO}_3\text{-PbSnO}_3$** 

Maria A. Kniazeva,<sup>1,\*</sup> Alexander E. Ganzha<sup>1</sup>, Irena Jankowska-Sumara<sup>2</sup>, Marek Paściak,<sup>3</sup> Andrzej Majchrowski<sup>4</sup>, Alexey V. Filimonov<sup>5,1</sup>, Andrey I. Rudskoy,<sup>1</sup> Krystian Roleder<sup>6</sup>, and Roman G. Burkovsky<sup>1,†</sup>

<sup>1</sup>*Peter the Great Saint-Petersburg Polytechnic University, 29 Politekhnicheskaya, 195251, St.-Petersburg, Russia*

<sup>2</sup>*Institute of Physics, Pedagogical University of Cracow, Podchorążych 2, 30-084 Krakow, Poland*

<sup>3</sup>*FZU–Institute of Physics of the Czech Academy of Sciences, Na Slovance 1999/2, 182 21 Prague 8, Czech Republic*

<sup>4</sup>*Institute of Applied Physics, Military University of Technology, ul. Gen. Kaliskiego 2, 00-908 Warszawa, Poland*

<sup>5</sup>*Alferov University, 8-3-A Khlopina, 194021, St.-Petersburg, Russia*

<sup>6</sup>*Institute of Physics, University of Silesia, 75 Pułku Piechoty 1, 41-500 Chorzów, Poland*



(Received 15 October 2021; accepted 29 November 2021; published 4 January 2022)

Perovskite solid solutions  $\text{PbHfO}_3\text{-PbSnO}_3$  offer valuable opportunities for studying the formation mechanisms of incommensurate phases, owing to the presence of an intermediate (between cubic and incommensurate) phase, which is stabilized in  $\text{PbHfO}_3$  upon  $\text{PbSnO}_3$  admixture. Here, an x-ray diffuse scattering signal is used to quantify the evolution of susceptibilities related to different modes of distortion (ferroelectric, incommensurate, antiferrodistortive) as a function of temperature and the results are critically compared to the predictions of a minimal symmetry-based Landau-like model with two coupled order parameters (ferroelectric and antiferrodistortive) and an incommensurate order parameter being interpreted as inhomogeneous polarization. Experimentally, we observe a Curie-Weiss-like linear dependence of ferroelectric stiffness (inverse of susceptibility related to homogeneous polarization fluctuations) in the cubic phase down to about 50 K above the transition to the intermediate phase, where this dependence nearly saturates. Upon cooling down to the intermediate phase, the maximum of susceptibility shifts gradually to the nonzero wave vector, where another Curie-Weiss-like linear stiffness trend is established, but with respect to the incommensurate order parameter. Symmetry of diffuse scattering distributions indicates an orthorhombic symmetry of the intermediate phase. A notable temperature dependence of the constant that describes the energy of polarization inhomogeneities is observed experimentally, which is in disagreement with the model expectations. The specifics of this dependence suggest the presence of a nearly temperature-independent characteristic length scale for inhomogeneities across several phases. Other differences with the model suggest that the incommensurate order parameter cannot be straightforwardly identified with weakly inhomogeneous ferroelectric polarization.

DOI: [10.1103/PhysRevB.105.014101](https://doi.org/10.1103/PhysRevB.105.014101)

**I. INTRODUCTION**

Antipolar ordering of cations in perovskite crystals attracts long time attention because of intrinsic scientific interest [1–3] and due to promising applications of antiferroelectrics [4–9]. These materials are a fruitful test ground for electron microscopy studies [10,11], scattering experiments [12–15], and theories [1,3,12,16–24]. A significant share of theoretical attention is given to interacting order parameters in  $\text{PbZrO}_3$ -like antiferroelectrics and to the mechanisms of incommensurate phases formation. This paper provides an experimental material related to those questions by reporting a diffuse scattering study of  $\text{Pb}(\text{Hf}_{0.7}\text{Sn}_{0.3})\text{O}_3$ . This crystal has an intermediate phase, where oxygen octahedral tilts are already developed, while the incommensurate order parameter exists only in the form of fluctuations. Studying those fluctuations by diffuse scattering helps in identifying the important order parameter interaction terms in a Landau-like phenomenological model

and register the incommensurate soft mode that has been experimentally elusive in crystals of this family.

**A. Models of antiferroelectrics**

Complexity of antiferroelectrics resulted in a rather large number of different approaches and perspectives in their modeling. To help the reader navigate that, a brief systematization follows.

The first model of antiferroelectrics is due to Kittel [1], who reduced an (at that time, abstract) antiferroelectric to two interpenetrating lattices with antiparallel polarizations. The most studied real antiferroelectric,  $\text{PbZrO}_3$ , is much more complex than that, in part due to the more complex dipole ordering  $\uparrow\uparrow\downarrow\downarrow$  [25], due to the possibility of alternative incommensurate orderings [10] and due to the presence of antiphase octahedral tilts as a second type of distortion [25], usually coexisting with the antipolar ordering of cations.

Modern models fall, roughly, into three categories. First, *ab initio* analysis [26–28] of the energy landscape at zero kelvin, sometimes extended to modeling of finite temperature behavior *via* molecular dynamics [23,29,30]. Usually this

\*kniazeva.maria225@yandex.ru

†roman.burkovsky@gmail.com

extension needs a parametrization of energy in terms of local ionic displacements around high-symmetry positions (often referred to as the second-principles approach). Alternatively, the energy can be parametrized not in local coordinates, but in normal-mode coordinates [18,23], which is not suitable for molecular dynamics, but allows some more immediately comprehensible insights into the energetics of the crystal, in particular into coupling of different degrees of freedom.

The second category, semiempirical atomistic models, is more multifaceted. In contrast to *ab initio*, these models contain assumptions and phenomenological parameters, which makes them more flexible for exploring narrow and specific effects. For example, the simplified lattice-dynamics model of Ref. [17] suggests an atomistic picture behind temperature-dependent avoided crossing of acoustic and optic phonon branches; the model of Ref. [3] points to universal collaborative coupling between octahedral tilts and antiferroelectricity; and the model of Ref. [19] suggests a mechanism of dipole wave commensuralization in the presence of flat and soft polarization branches. More recently, Ref. [20] explores the link between bilinear coupling and incommensurate structures, and Ref. [22] shows how such structures can arise due to the dipole-dipole interactions, in analogy with polarization catastrophe in ferroelectrics.

The third category is Landau-like models, similar to that of Devonshire for BaTiO<sub>3</sub> [31]. These models do not account for the specifics of atomic structure and short-range interactions (in contrast to long-range electric and elastic effects [32]), but parametrize macroscopic thermodynamic potential based on symmetry arguments. In contrast to Landau theory of second-order phase transitions [33], Landau-like models do not claim exactness in any applicability domain [34], but often describe the experimental observations adequately.

For antiferroelectric perovskites, such an approach was applied by Haun *et al.* [16], who have reproduced electric and elastic behavior in PbZrO<sub>3</sub> by a model with ferroelectric and antiferroelectric order parameters coupled to each other and to the stress. Those parameters were considered homogeneous. Toledano and Khalyavin considered a similar model, but with coupling also to antiphase octahedral tilts [35]. Tagantsev *et al.* [12] proposed a Landau-like model for the same crystal where antipolar displacements correspond not to the independently defined antiferroelectric order parameter (as in Haun's work), but to inhomogeneous polarization. Additionally, that model accounts for inhomogeneous strain, acousto-optic (flexoelectric) coupling, umklapp interactions, and biquadratic coupling between acousto-optic waves and antiphase octahedral tilts.

Presently there is no consensus on why the PbZrO<sub>3</sub>-like crystals tend to be incommensurate instead of ferroelectric. The proposition of Tagantsev *et al.* [12] that it is due to flexoelectric interaction is in line with a broader discussion on the possible origin of incommensuration in dielectrics [36–38] due to the presence of an invariant term of the form  $P\partial u/\partial x - u\partial P/\partial x$ , where  $P$  is the polarization and  $u$  is the strain or another quantity with appropriate transformational properties. A point of confusion in that broader discussion has been summarized by Blinc and Levanyuk [36] as follows: “In the literature one may find the assertion that it is this coupling, which is a general reason for [incommensurate]

phase formation. Such a statement would be meaningful only if one could be sure that the nonrenormalized coefficient [of polarization correlation energy] is positive. But we hardly know confidently if it is the case...”. A recent step towards a better understanding of that is the work by Stengel [39], where the applicability of a continuum model with flexoelectric coupling has been analyzed in connection to describing the *ab initio*-derived phonon dispersion curves of SrTiO<sub>3</sub>. That work suggests that a continuum description can be adequate, but needs to be more complex than usually considered [40,41]. Extension of the improved continuum model towards free-energy analysis of antiferroelectrics at high temperatures has not yet been attempted. There are few microscopic models in the literature [20,22,42] that suggest a way of obtaining the negative *nonrenormalized* coefficient above due to particular atomic-level specifics of perovskites. This ambiguity seems presently distant from the resolution.

## B. Motivation

There is a considerable experience of simulating polarization fluctuations, as seen by scattering, in the cubic phase of perovskites [43,44], where there are no other order parameters with which the polarization could interact. When the symmetry becomes lower than cubic, the goal becomes more complex [14]. The positive side of that complication is, however, an emerging possibility of studying the energetics of order parameter interactions in low-symmetry phases.

A natural test ground for this could be the high-pressure intermediate phase in PbZrO<sub>3</sub> [14,45] and PbHfO<sub>3</sub> [45,46] that becomes stable between the cubic and the incommensurate phases almost immediately on raising pressure above ambient. This phase of lower-than-cubic symmetry has an order parameter (octahedral tilts, as Ref. [46] suggests), apparently no long-range ordered displacements in the cation subsystem, but strong fluctuations of inhomogeneous polarization, as seen by diffuse scattering. It would be seen as a good model object, but studying it in temperature domain is difficult, since pressure complicates such experiments considerably. A possible strategy is to study a similar phase, but created, somehow, without pressure; for example, by chemical modifications.

## C. Tin-doped PbZrO<sub>3</sub> and PbHfO<sub>3</sub>

It is instructive to consider tin-doped PbZrO<sub>3</sub> and PbHfO<sub>3</sub>. In contrast to titanium doping, which leads to ferroelectric lead zirconate titanate [47], doping by tin leads in a completely different direction [48]. Tentatively, the fully filled  $d$  shell of tin prevents it from acting like titanium, but results in effect similar to that of pressure due to ionic radius difference. As a result of tin doping the intermediate phase forms, appearing highly similar to the one(s) under pressure.

In the parent compound of PbHfO<sub>3</sub>-PbSnO<sub>3</sub>, pure PbHfO<sub>3</sub>, two phase transitions occur on varying temperature: at about 163 °C, the low-temperature antiferroelectric (AFE1) phase [49] transforms to the incommensurately modulated AFE2 phase [15,44,50], and at about 215 °C the cubic phase forms. Curiously, cubic  $\rightarrow$  AFE2 transition is a triggered incommensurate transition, which is controlled not by an

incommensurate soft mode, as in most of the incommensurate dielectrics [36], but by the softening of the antiferrodistortive (AFD) mode [44]. The triggered transition scenario is, seemingly, suppressed on doping by tin, because an intermediate phase between the cubic and the AFE2 phases appears, allowing the distortions related to the AFD and incommensurate order parameters to form at different temperatures [51]. There is no sharp drop in the dielectric constant in the intermediate phase [48] compared to the cubic phase, which suggests the intermediate phase to be nonpolar.

#### D. This work

This paper reports on a study of the intermediate phase and related transitions by diffuse scattering in  $\text{PbHfO}_3\text{-PbSnO}_3$  solid solution with 30% concentration of tin atoms – a nearly critical concentration in terms of solubility.

The primary observation is a strongly temperature-dependent incommensurate diffuse intensity maximum in the intermediate phase, which emerges gradually from zone-center maximum in the cubic phase. To put that into a quantitative basis, we propose recalculating intensities to stiffness with respect to distortions, in which case the situation becomes more understandable. This leads to further notes, such as unusual saturation of dielectric stiffness in cubic phase and a surprisingly linear (Curie-Weiss) trend for incommensurate stiffness going to zero at the point of incommensurate transition.

Particularly interesting is the behavior of correlation energy, which characterizes how much the crystal resists inhomogeneities in polarization. In contrast to what is expected for normal ferroelectric crystals, the one under study has a notably temperature-dependent correlation energy, not only in the intermediate phase, where, as we suggest, interaction between its order parameter (tilts) and polarization gradient could explain that, but also in the cubic phase, where it occurs spontaneously. This temperature dependence of correlation energy suggests a possibility of an unusual, largely temperature-independent characteristic length scale for inhomogeneities.

The findings help in advancing the experimental and interpretation methodology, as well as add some particular physical insight, especially on the interaction of octahedral tilts and dipoles arrangement.

## II. METHODS

### A. Experiment

Single crystals of  $\text{PbHfO}_3\text{-PbSnO}_3$  have been grown by a spontaneous crystallization method at Institute of Applied Physics MUT, Warsaw, Poland, as described in Ref. [48]. Experiments on diffraction and diffuse scattering have been performed at the European Synchrotron Radiation Facility (ESRF), at the side station of ID28 beamline. For measurements we have used a needlelike piece with a cross section of about  $100 \times 100$  microns, mounted on quartz capillary and heated in the flow of hot air from a heat blower. The measurements were done in a cooling cycle. Tight focusing of the beam ( $\sim 40 \mu\text{m}$ ) and the relatively large size of the sample, as compared to the characteristic attenuation length

of  $\sim 10.5 \mu\text{m}$  (wavelength of  $\lambda = 0.6968 \text{ \AA}$ ), induced a considerable inhomogeneity in the overall signal distribution in reciprocal space, prompting us to analyze the data corresponding to a sufficiently homogeneous part of it. The exposure was 0.2–0.5 s per  $0.1^\circ$  angular step. Data treatment has been carried out using the CRYSTALIS PRO program and custom-built MATLAB codes.

### B. Interpreting and modeling the signal

Diffuse scattering (DS) is a scattering corresponding to wave-vector transfers,  $\vec{Q}$ , that are outside the reciprocal lattice points,  $\vec{\tau}$ . It is due to disorder in the arrangement of scattering centers, which in the case of crystals under study corresponds, mainly, to partially disordered, but still correlated displacements of ions from their nominal positions in the structure.

DS from fluctuations of a particular normal mode (order parameter) is proportional to susceptibility, according to the formula [52]

$$I(\vec{Q}, T) = T \cdot |F_{\text{DS}}(\vec{Q})|^2 \cdot \chi(\vec{q}, T), \quad (1)$$

where  $T$  is the temperature in energy units,  $F_{\text{DS}}$  is the structure factor for diffuse scattering, and  $\chi = \alpha^{-1}$  is the susceptibility with respect to that normal mode. The structure factor  $F_{\text{DS}}$  is computed similarly to the inelastic structure factor for scattering by phonons [52,53]. Relatively simple cases of the present paper (transverse polarization waves and tilts of octahedra around a particular axis) can be treated with a simplified form for the structure factor

$$F_{\text{DS}} \sim (\vec{Q}\vec{u}_{\vec{q}}), \quad (2)$$

where  $\vec{u}_{\vec{q}}$  is the Fourier component of displacements distribution, corresponding to reduced wave vector  $\vec{q} = \vec{Q} - \vec{\tau}$ . This simplification is obtained (see Appendix) by neglecting the interference of scattering centers within the cell, but keeping the essential dependence on the directions of displacements.

This approach to probing stiffness with respect to a particular normal mode is enabled by the following general relationship between stiffness and fluctuations:

$$\langle P^2 \rangle = \frac{T}{\alpha}, \quad (3)$$

where  $\langle P^2 \rangle$  is the ensemble averaged square of normal mode amplitude,  $P$ . This follows from the equipartition theorem, stating that the average thermal energy deposited into a normal mode in equilibrium,  $\alpha \langle P^2 \rangle / 2$ , equals to  $T/2$ . The diffuse scattering signal due to that normal mode is proportional to  $\langle P^2 \rangle$ , so  $\alpha$  can be extracted upon taking into account the corresponding structure factor, provided that the relevant signal is separated from other scattering.

This stiffness is the same as the one determining linear response to a conjugate field,  $E$ , as

$$P = \alpha^{-1} E. \quad (4)$$

If  $P$  is polarization and  $E$  is the electric field (any order parameter and conjugate field can be substituted here), then  $\alpha^{-1}$  should be dielectric susceptibility, as measured in capacitors. This links scattering measurements, sensing temperature-induced  $\langle P^2 \rangle$ , to linear response measurements, sensing  $P$  as a function of  $E$ .

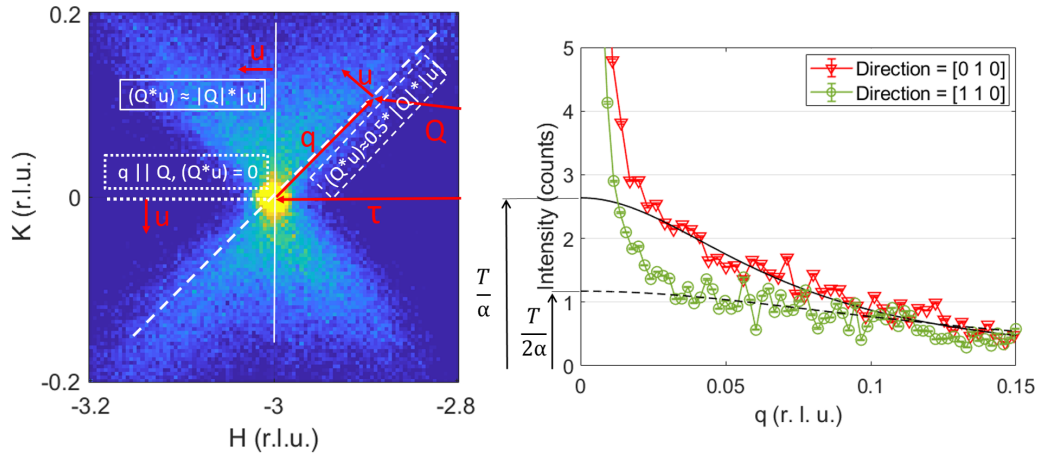


FIG. 1. Schema of determining the stiffness with respect to transverse polarization waves in the cubic phase. Intensity along  $\tau$  corresponds to the background (which is subtracted from profiles), because of zero structure factor for transverse waves. Stiffness at the zero wave vector is obtained by fitting a finite-wave-vector signal using a Lorentzian line shape. Such fits along different directions provide mutually consistent estimates of  $\alpha(\vec{q} = 0)$ .

Stiffness with respect to a particular order parameter, when considered as a function of the wave vector, should be parabolic near  $q = 0$ :

$$\alpha(\vec{q}) = \alpha + \sum_{i,j} D_{i,j} q_i q_j, \quad (5)$$

which reflects that a homogeneous order parameter should be energetically less expensive than an inhomogeneous one (as long as there is no Lifshitz invariant, which holds for cubic perovskite structure). Therefore, when considering an arbitrarily oriented line in reciprocal space going through a reciprocal space node, one should expect a Lorentzian-shaped intensity profile

$$I(\vec{Q}) \sim \frac{T |F_{\text{DS}}(\vec{Q})|^2}{\alpha + D_2 |\vec{q}|^2}, \quad (6)$$

where  $D_2$  is a constant of spatial correlation energy for that order parameter along that direction. In the case of polarization waves, one should count  $\vec{q}$  as originating at the cubic  $\Gamma$  points, while in the case of oxygen octahedral tilts, one should treat it as originating from the  $R$  points. Basically, the data treatment proceeds by experimentally quantifying the parameters in formula (6) and, in the less trivial cases, beyond it. An annotated example of extracting the dielectric stiffness from diffuse scattering in cubic phase is shown in Fig. 1.

Note that this approach can be justified only near the parent Bragg reflections with small structure factor. Small structure factor for Bragg scattering implies small structure factor for scattering by long-wavelength acoustic waves. This allows sensing mostly distortions of the cells, while the shifts of the cells as a whole are discarded to a large degree. For that purpose, this work uses  $(-3, 0, 0)$  Bragg peak, which has a relatively small structure factor, about 1/10 of that for the strong  $(2, 0, 0)$  peak.

The diffuse scattering data of the present work are treated as if the scattering originated from fluctuations of inhomogeneous polarization only. In fact, these waves may be “renormalized” due to flexoelectricity or other similar-in-

form interactions (see Introduction) and contain, therefore, a mixture of polarization and some other property. This possibility is ignored in direct data modeling of the present work, mainly because the data do not allow distinguishing one possible renormalization scenario from the other. It is assumed that the present data treatment results could be reassessed upon obtaining a more specific understanding of renormalization in the future.

Order parameter magnitudes are seen in diffraction by intensities of superstructure reflections. When distortions are small, these intensities are proportional to the square of the distortion magnitude [52]. So, if the transition is of second order, one expects nearly linear temperature dependence of intensities,  $I \sim (T_0 - T)$ , without discontinuities. In the first-order transition case, one expects a jump at the transition temperature.

### III. RESULTS

#### A. Two phase transitions

The range of temperatures that have been studied contains three different phases: incommensurate phase (AFE2), intermediate phase (IM), and the cubic phase. Their characteristic scattering patterns are shown in Fig. 2. The low-symmetry AFE2 phase shows incommensurate reflections at  $\Sigma_F$  ( $h \pm \xi_F, k \pm \xi_F, l$ ) points and zone-boundary reflections at  $R$  ( $h + 0.5, k + 0.5, l + 0.5$ ) points, which is consistent with structural reports on the same phase in pure  $\text{PbHfO}_3$  [15,50]. In the higher-temperature IM phase, the sharp reflections at  $\Sigma_F$  disappear, while diffuse scattering maxima about the same positions emerge.

As to the  $R$ -point reflections in the IM phase, they demonstrate a particular systematics. All the inspected (few tens) reflections at the  $R$  points with symmetric indices,  $|H| = |K| = |L|$ , are by about an order of magnitude less intense than some of the reflections with nonsymmetric indices. From this one may suggest that the  $R$ -point reflections are mostly due to the octahedral tilts. If they were totally due to the tilts,

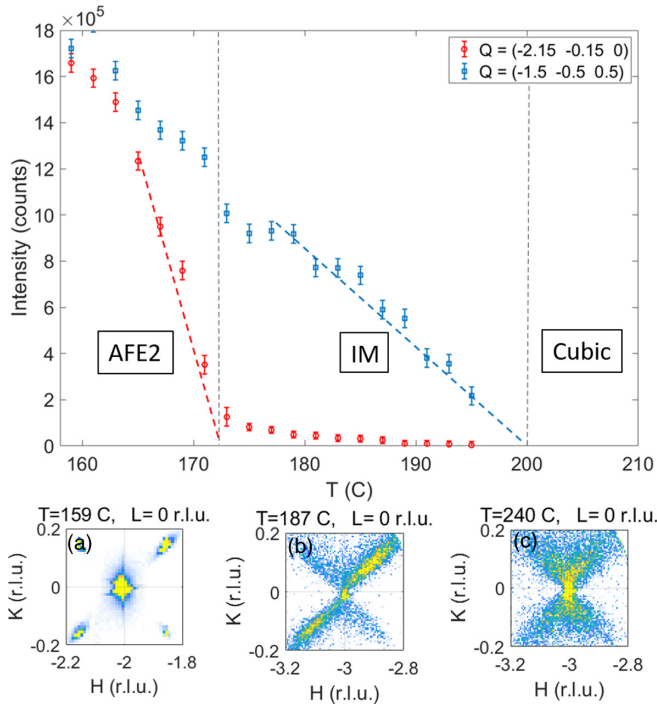


FIG. 2. Three phases of  $\text{Pb}[\text{Hf}_{0.7}\text{Sn}_{0.3}]\text{O}_3$ : incommensurate AFE2 (a), intermediate IM (b), and cubic (c). Squares: intensity at  $R$ -points; circles: intensity of  $\Sigma_F$  reflections. Nonzero values above the IM-AFE2 transition are due to the intensity of diffuse scattering at the incommensurate positions. Dashed lines show the transition temperatures.

the symmetric reflections would be expected totally absent in the small-displacement limit [54]. The experimental presence of small intensities at symmetric  $R$  points can be attributed to the minor presence of an additional distortion mode (such as antiphase Pb shifts) or to the violation of small-displacement limit in the experiment. Tentatively, the octahedral tilt pattern is the same as in the AFE1 and AFE2 phases ( $a^-a^-c^0$ ), but with smaller amplitude.

In the cubic phase, there are no superstructural reflections, and diffuse scattering has a butterflylike shape with a maximum at the center of the Brillouin zone.

From scattering, both transitions appear to be close to the second order. Intensities of the corresponding superstructural reflections increase linearly directly near the transition temperatures. It seems most natural to estimate the transition temperatures by extrapolating the linear sections to the temperature axis,  $T_{\text{AFD}} \approx 200^\circ\text{C}$  and  $T_{\text{IC}} \approx 172^\circ\text{C}$ .

### B. Antiferrodistortive mode critical dynamics

Since the transitions appear close to the second order, a critical increase of respective susceptibilities should occur on approaching the transition temperatures. That should manifest in diffuse scattering intensity increase at and near the corresponding points of the Brillouin zone, which is, for AFD tilting, the  $R$  point.

Diffuse cross-shaped distributions (Fig. 3) are formed by the intersecting diffuse scattering rods oriented along the  $H$ ,

$K$ , and  $L$  directions. There are very weak or no rods for which  $\vec{q} = \vec{Q} - \vec{Q}_R$  is approximately parallel to  $\vec{Q}$ . Consequently, the displacements from which the scattering stems are perpendicular to  $\vec{q}$ . Taking into account that we consider antiphase tilts, the tilts are around the direction of  $\vec{q}$ . Visually, such an inhomogeneous fluctuation in tilt subsystem can be imagined as in Fig. 4. As the cubic  $\rightarrow$  IM transition is approached, the intensity of the rods increases, as can be seen from the profiles. Unexpectedly, the intensity of the rods drops sharply at  $T = 220^\circ\text{C}$ , which is still significantly higher than the transition temperature obtained from the extrapolation of the amplitude of the tilting ( $T = 200^\circ\text{C}$ ).

In the language of stiffness, this corresponds first to its gradual decrease on cooling and then, in an abrupt increase at  $T = 220^\circ\text{C}$  [Fig. 5(a)].

If one inspects not the extrapolation of DS intensity to the  $R$  point, but the integrated intensity in its vicinity, then the picture becomes different [Fig. 5(b)]. Integral intensity grows without unexpected features. The reason is that at a temperature where diffuse scattering is suppressed ( $T = 220^\circ\text{C}$ ) the sharp peak at the  $R$  point itself increases strongly (it is still much weaker than in the IM phase), and the total intensity nevertheless increases. Upon recalculating this integral intensity value into a stiffness, the resulting effective stiffness behaves as expected; it decreases on approaching the transition [dashed line in Fig. 5(a)].

It is natural to explore how it looks from the perspective of tilt-tilt correlation length [Fig. 5(d)]. The formula for this quantity,  $\Lambda = \sqrt{D_2}/\alpha_{\text{AFD}}$ , is extracted from the denominator of Eq. (6) as the combination with dimension of length. At temperatures that are above diffuse intensity drop, the length grows on cooling, agreeing with the theoretical expectations, which are shown by dashed lines [Fig. 5(d)]. At the moment of diffuse intensity drop, the length also decreases sharply. It turns out that the correlation length associated with normal diffuse scattering does not grow significantly higher than 20–30 cells. On the other hand, the continued growth of the integral intensity, and, in particular, the narrow Bragg-like component directly at the  $R$  point, suggests that the degree of ordering of the tilting still grows further. It is likely that for an adequate assessment of the stiffness and correlation length it is necessary to take into account both the normal diffuse signal (Lorentzian-like) and the narrow component directly at the  $R$  point. At the moment, it is not clear how this should be made most consistently (we used intensity integration as the simplest approach). Parallels can be seen with phonon spectroscopy, where energy integration with taking into account also the central peak, appears necessary to estimate the “true” stiffness [44,55].

An alternative suggestion could be that maybe the sample at  $T = 220^\circ\text{C}$  is not fully homogeneous and some subvolumes of it are already in the ordered (IM) phase, while the rest of the crystal is in cubic phase. The Bragg-like component is, in this case, just a normal Bragg reflection from those ordered regions. In the case of  $\text{SrTiO}_3$  a similar question arose (see Ref. [52], Sec. III.2.1, for review) and was the subject of targeted studies [56], which were aiming at elucidating the possibility of higher transition temperature in near-surface layers, but did not confirm that.

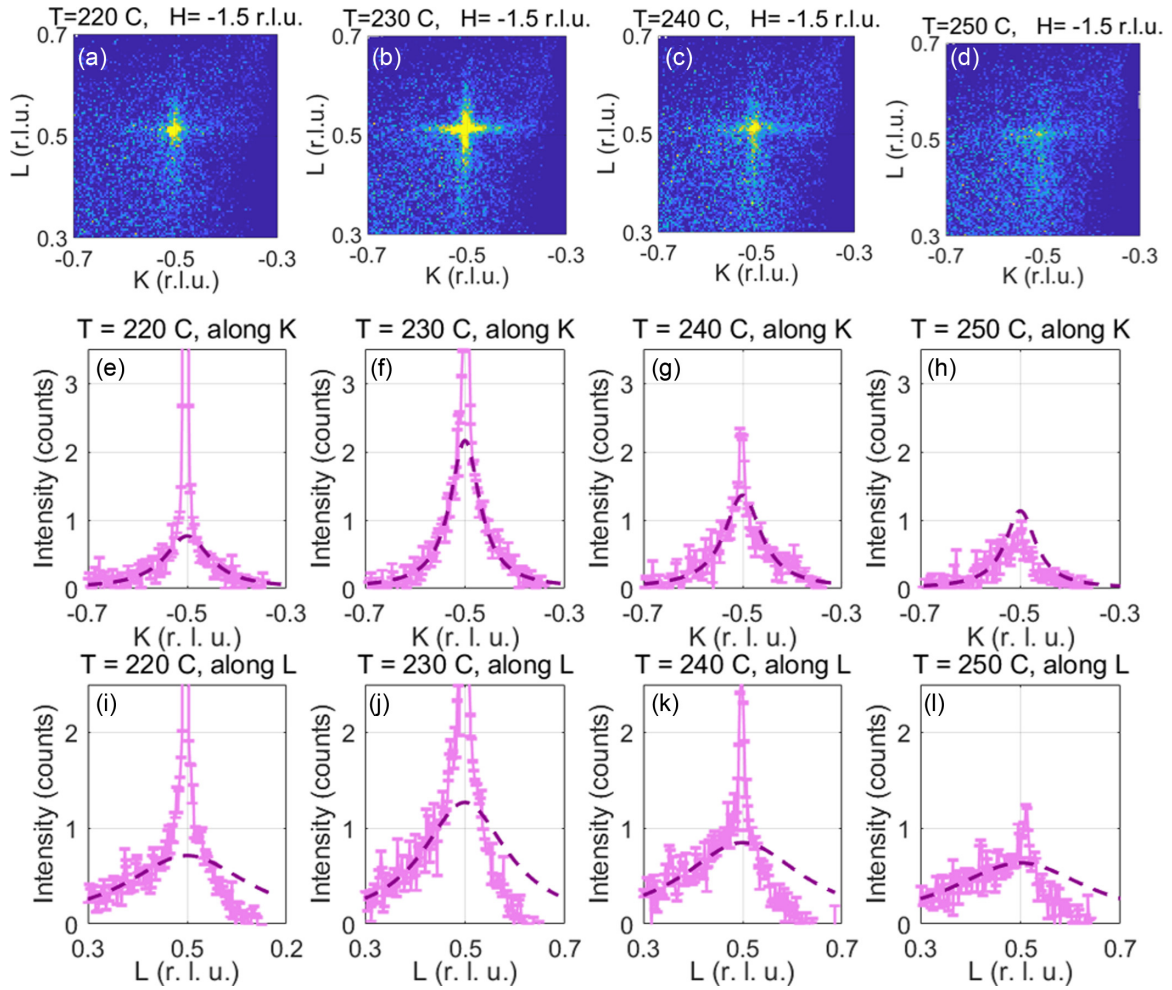


FIG. 3. Diffuse scattering distribution in the vicinity of the  $(-1.5 -0.5 0.5)$  reflection in the cubic phase. Profiles (e)–(l) are constructed by integrating the signal in cylinders with a radius of 0.014 reciprocal lattice units (r.l.u.). Dashed lines are the fit by Lorentzian  $I = \frac{T}{\alpha + D_2(\vec{q} - \vec{q}_0)^2}$ . Asymmetry of the  $L$ -direction profile is likely due to the experimental artifact: in some places of the reciprocal space there are strong intensity gradients due to the relatively large size of the sample in comparison with the characteristic absorption length of radiation in it.

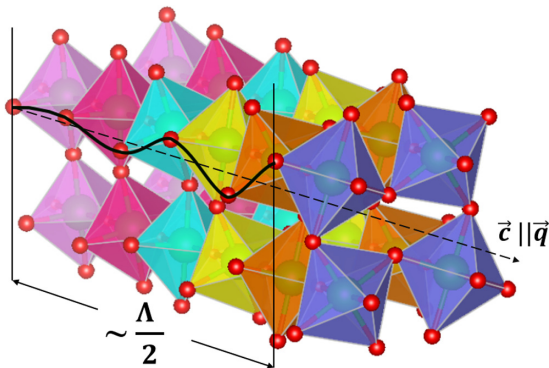


FIG. 4. A real-space view of an AFD fluctuation responsible for diffuse scattering rods near  $R$  points. Octahedra experience antiphase tilts around the axis that coincides with the direction of the wave vector, i.e., the direction in which the pattern slowly changes in real space. In the present case, this change is assumed as just the decay of tilt magnitude over the characteristic correlation length,  $\Lambda$ . Note that this pattern of short-range tilt correlations is similar to  $a^0 a^0 c^-$ , which is different from the tilt pattern in the antiferroelectric, incommensurate, and (presumably) IM phases, which is  $a^- a^- c^0$ .

### C. Unrealized transition to the polar phase

In addition to an increase in the AFD susceptibility, an increase in the dielectric susceptibility is also expected in the cubic phase, according to the dielectric studies of  $\text{Pb}(\text{Hf}_{0.7}\text{Sn}_{0.3})\text{O}_3$  crystals [48].

The stiffness at  $\vec{q} = 0$ , denoted as  $\alpha_{\text{FE}}$  and determined by the fitting of diffuse scattering profiles (Fig. 6), decreases on cooling (Fig. 7). At high temperatures (300–450 °C) this fits to the Curie-Weiss law with a critical temperature  $T_{\text{FE}} \approx 200$  °C, which coincides unexpectedly well with the AFD transition temperature. At lower temperatures (220–250 °C) the stiffness decrease slows down, and nearly saturates. This lower-temperature saturation seems qualitatively compatible with the dielectric data of Ref. [48], which is coplotted. The absence of divergence of susceptibility at zone center agrees well with the absence of ferroelectric transition (AFD transition occurs instead).

### D. Incommensurate mode critical dynamics

Since the transition from the IM phase to the AFE2 phase is incommensurate, it is logical to expect a decrease in the

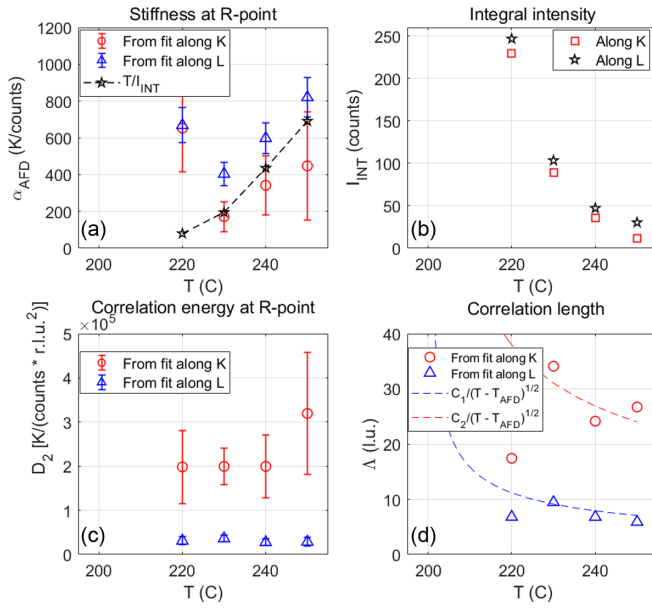


FIG. 5. Diffuse scattering parameters in the vicinity of the  $R$  point  $(-1.5 -0.5 0.5)$ : (a) AFD stiffness  $\alpha_{\text{AFD}}$  determined by independent fits along the  $K$  and  $L$  axes. We think that the true stiffness, which does not depend on the direction in cubic phase, is the average between them. Stars are the stiffness recalculated from the integral intensity of the profiles along  $L$ . (b) Integral intensity for the corresponding directions. (c) Correlation energy constant  $D_2$ . (d) Correlation lengths of displacements recalculated from stiffness and correlation energy constant. Dashed lines are theoretical expectations under the assumption  $D_2 = \text{const}$  and  $\alpha_{\text{AFD}} = A(T - T_{\text{AFD}})$ .

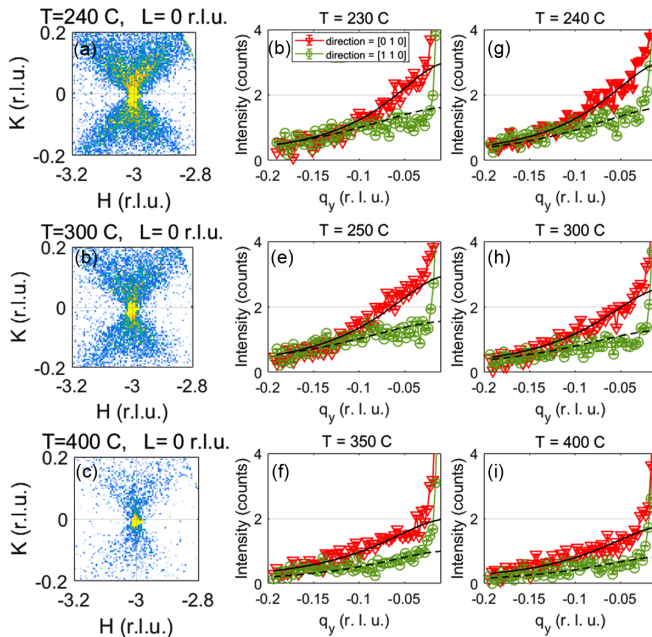


FIG. 6. Distribution of diffuse scattering in the cubic phase. Two-dimensional distributions (cuts through  $Q = (-3 0 0)$  by  $H K 0$  plane) are shown using same color scale. The profiles correspond to  $[1 1 0]$  (circles) and  $[0 1 0]$  (triangles) directions, background subtracted. Solid and dashed lines are fit by Lorentzian  $I = \frac{T}{\alpha + D_2(\bar{q} - \bar{q}_0)^2}$ .

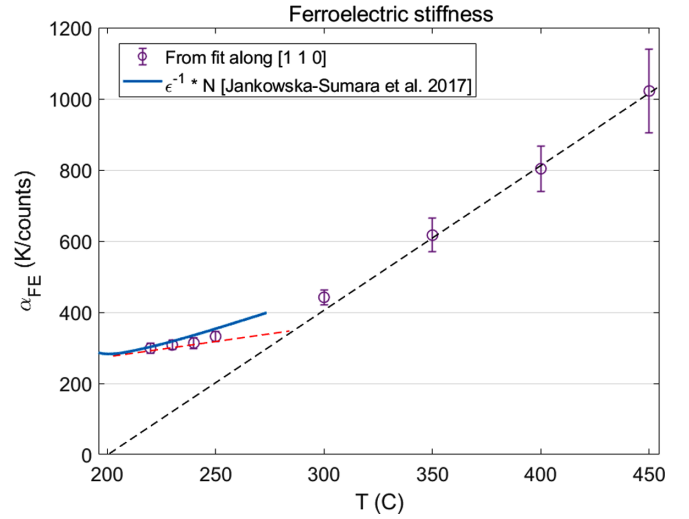


FIG. 7. The temperature dependence of the dielectric stiffness, determined by the analysis of diffuse scattering in the cubic phase compared to dielectric measurements [48]. For a correct comparison, the moment of the phase transition of the dielectric data was shifted in temperature to the value  $T = 200^\circ\text{C}$  at which a phase transition is observed in the current study.

stiffness corresponding to transverse incommensurate waves. Indeed, we register a minimum of stiffness  $\alpha_{\text{IC}}$  at an incommensurate position,  $q_0$ . This can be seen from the scattering profiles [Figs. 8 and 9(a)], where the maximum is located in the vicinity of  $q_0 = (0.15, 0.15, 0)$ . The position of the maximum shifts away from the center of the zone as the sample cools down [Fig. 9(c)].

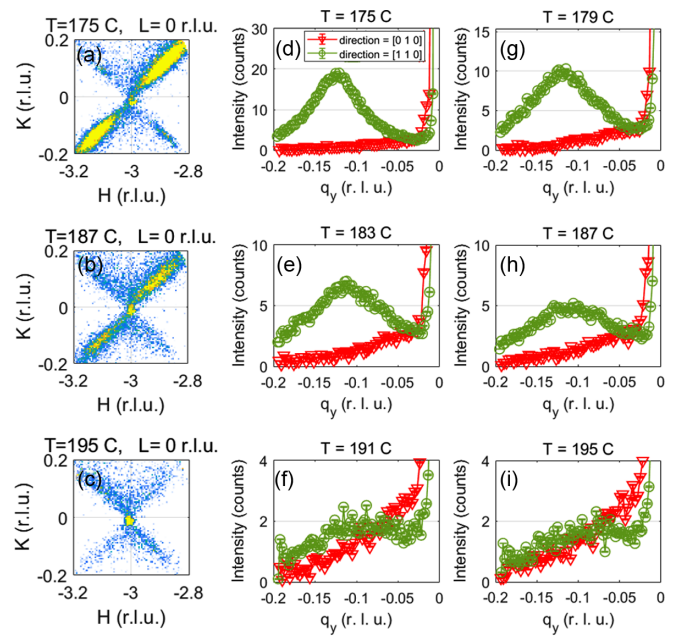


FIG. 8. Diffuse scattering distributions in the IM phase. Two-dimensional distributions [cuts through  $Q = (-3 0 0)$  by  $H K 0$  plane] are shown using the same color scale. The profiles correspond to  $[1 1 0]$  (circles) and  $[0 1 0]$  (triangles) directions, background subtracted.

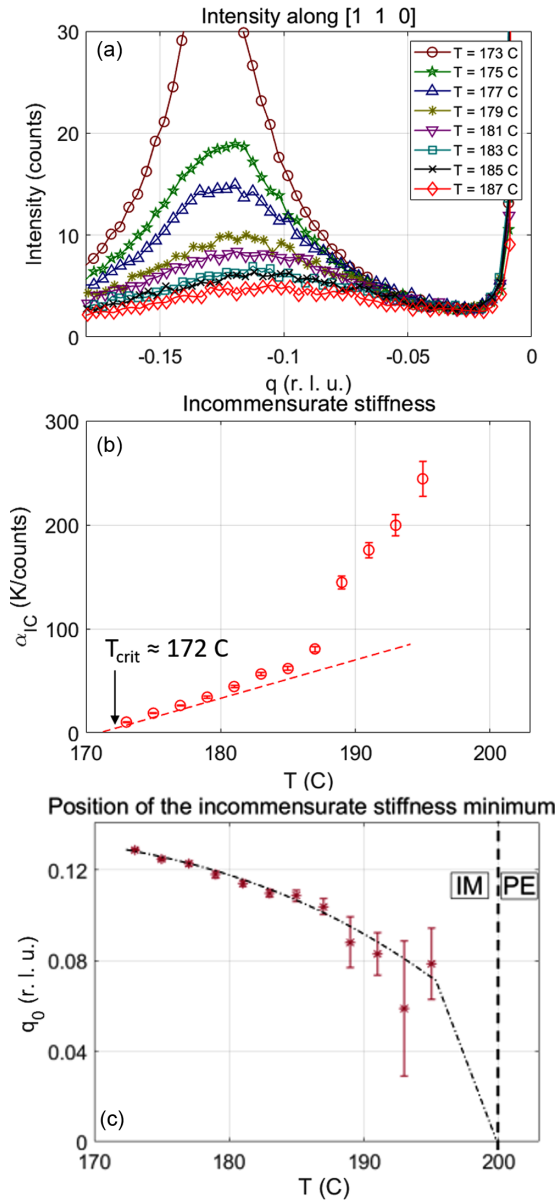


FIG. 9. Temperature dependence of the incommensurate diffuse scattering in the IM phase (a) and its parameters: incommensurate stiffness, measured as  $T/I_{\max}$  (b), and the position of intensity maximum (c).

The most interesting feature of this maximum is that the incommensurate stiffness, recalculated from its amplitude, behaves linearly when approaching the IM  $\rightarrow$  AFE2 transition and the critical temperature for this linear dependence coincides with the transition temperature [Fig. 9(b)]. At the same time, the position of the minimum of the stiffness just above the transition coincides with the position of the incommensurate reflection just below it. These two factors are consistent with what would be expected from classical soft-mode-driven (second-order) incommensurate transition [36]. However, this apparent similarity to second-order transition does not directly agree with the presence of nonzero latent heat in calorimetric measurements of such crystals [48]. This discrepancy is of interest, although no immediate explanation is apparent, apart

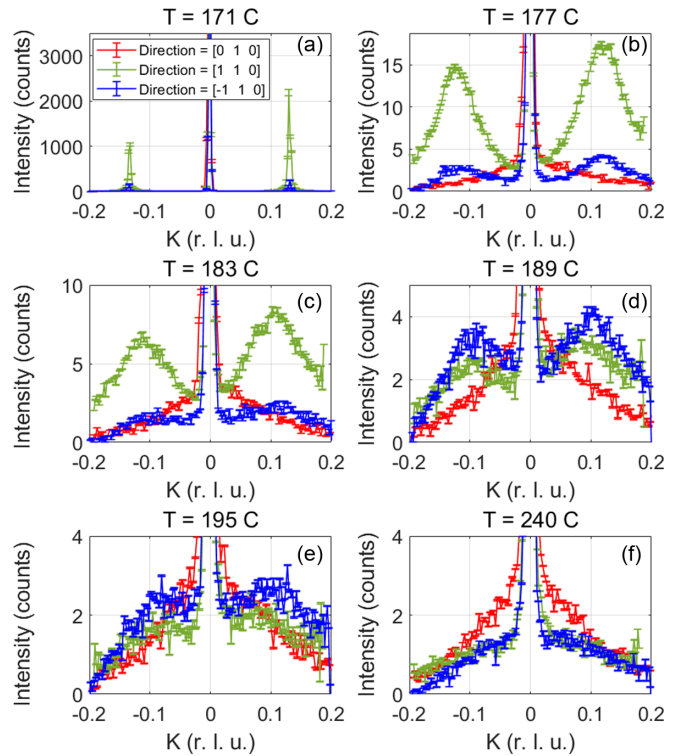


FIG. 10. Population of domains in the AFE2 and IM phases. In the AFE2 phase (a), as well as in the low-temperature region of the IM phase (b), (c), domains with incommensurate maxima along the  $[1\ 1\ 0]$  direction strongly prevail in volume over domains with incommensurate maxima along the  $[-1\ 1\ 0]$  direction, and other directions (not shown). However, as the transition to the cubic phase is approached, the intensities along the  $[1\ 1\ 0]$  and  $[-1\ 1\ 0]$  directions are equalized (d), (e). Cubic phase (f) shows equal intensities in these directions.

from a possibility that the experimentally registered latent heat is due to extrinsic sources, such as domain redistribution at the transition point.

The linear trend of incommensurate stiffness breaks at  $T = 188^\circ\text{C}$ , where the slope changes [Fig. 9(a)]. Seemingly, this is due to a change in the distribution of IM-phase domains with different orientations at  $T$  about  $187\text{--}189^\circ\text{C}$ , as Fig. 10 indicates.

## IV. INTERPRETATION

Here, a symmetry-guided minimal Landau-like model is built and the experimental data are compared to its predictions.

### A. Symmetry of the IM phase

The structure of the IM phase has not yet been refined crystallographically. However, plausible assumptions on it can be made on the basis of its AFD character, general symmetry considerations, and experimentally observed symmetry of diffuse scattering.

The first candidate for an IM-phase unit cell is the orthorhombic one defined by vectors  $\vec{a}_{\text{IM}} = (a_{\text{PC}}, -a_{\text{PC}}, 0)$ ,  $\vec{b}_{\text{IM}} = (a_{\text{PC}}, a_{\text{PC}}, 0)$ ,  $\vec{c}_{\text{IM}} = (0, 0, 2a_{\text{PC}})$ , where  $a_{\text{PC}}$  is the



pseudocubic lattice parameter. Oxygen octahedra are tilted in an  $a^-a^-c^0$  pattern around  $\vec{a}_{\text{IM}}$ . Such a cell of  $Imma$  symmetry has been considered by Tolédano and Khalyavin [35] (axes  $a$ ,  $b$ , and  $c$  assigned differently in the present work to have them similar to those in the AFE phase) as a virtual intermediate structure between cubic and antiferroelectric structures. Also, this cell corresponds to the average structure of the incommensurate phase of  $\text{PbHfO}_3$ , as determined crystallographically [15].

The orthorhombic  $Imma$  cell is compatible with the observed symmetry of diffuse scattering. This can be deduced as follows. If one considers a temperature near the bottom of the IM phase stability range, like  $T = 177^\circ\text{C}$ , the diffuse scattering maxima along the  $[1\ 1\ 0]$  direction are five to seven times more intense than those along  $[1\ -1\ 0]$ ,  $[1\ 0\ 1]$ , and  $[1\ 0\ -1]$ . Intensity profiles along  $[1\ 1\ 0]$  and  $[1\ -1\ 0]$  are shown in Fig. 10(b), while the latter two directions ( $[1\ 0\ 1]$  and  $[1\ 0\ -1]$ ) are omitted for clarity of the figure; the intensity of the respective profiles is about the same as along  $[1\ -1\ 0]$  at this temperature. It is possible to verify that such a combination of intensities cannot be reproduced by any combination of rhombohedral-symmetry domains or tetragonal-symmetry domains, but is compatible with orthorhombic-symmetry domains. The volume shares of different orientational domain states are changing with temperature, as commented in the caption of Fig. 10.

## B. Minimal Landau-like model of the IM phase

By knowing (actually, reliably guessing) the order parameter of the IM phase, it is possible to learn how the stiffness landscape in wave-vector space should be organized. The order parameter is assumed to be  $\vec{\eta}_0 = \eta_0(\frac{1}{\sqrt{2}}, \frac{1}{\sqrt{2}}, 0)$ : antiphase tilts around  $\vec{a}_{\text{IM}}$ . The idea is to build such a symmetry-determined free-energy expansion, in which by means of the lowest-possible-order terms involving  $\vec{\eta}_0$  and polarization gradients, the key specifics of the IM phase are accounted for.

### 1. Cubic part of the free-energy expansion

Free energy of inhomogeneous polarization in a cubic crystal is given as [57]

$$F_P = \frac{\alpha}{2} \vec{P}^2 + \frac{1}{2} \sum_{i,j} D_{ijlm} \frac{\partial P_i}{\partial x_i} \frac{\partial P_l}{\partial x_m}, \quad (7)$$

where  $\vec{P}$  is polarization,  $\alpha$  is dielectric stiffness,  $D_{ijlm}$  is polarization correlation energy tensor, and  $x_i$  is coordinates  $x$ ,  $y$ , and  $z$ . This formula does not account for the LO-TO splitting due to the long-range electrostatic interactions, which should be, in principle, included in such macroscopic consideration [32]. Here, for simplicity, we do not consider them, but instead (which is largely equivalent) just assume that all possible polarization waves in Eq. (7) are transverse.

### 2. Interaction between polarization and tilts

Interaction of polarization with  $\vec{\eta}_0$  should be described by those coupling terms between  $\Gamma_4^-$  (for polarization) and  $R_4^+$  (for tilts) distortions that the cubic symmetry allows. The Supplemental Material [58] lists such terms up to fourth order

(and up to second order in gradients), as provided by ISOTROPY software [59].

The commonly considered coupling is the biquadratic coupling [12,60], which is represented by three fourth-order terms. In our case they are proportional, respectively, to

$$(P_x^2 + P_y^2)\eta_0^2, P_x P_y \eta_0^2, \text{ and } P_z^2 \eta_0^2. \quad (8)$$

This biquadratic coupling between  $\vec{\eta}_0$  and homogeneous polarization accounts for the change in the dielectric tensor between the cubic and IM phases, but does not account for the change in spatial correlations of polarization.

### 3. Biquadratic coupling of tilts to polarization gradient

Spatial correlations should be affected by coupling terms involving polarization gradients. Also those terms should not contain  $\vec{\eta}_0$  gradients, because those should be zero for constant  $\vec{\eta}_0$ . Lowest-order terms of this sort are degree-3 terms linear in polarization gradient, which vanish in a big crystal, because their volume integrals are transformed to surface integrals of finite vector fields [33]. Therefore, the desired lowest-order interaction should be described by biquadratic terms between polarization gradients and homogeneous tilts, of which there are 30 invariants (only 15 are nonequivalent in big crystals) with terms proportional to [58]

$$\frac{\partial P_i}{\partial x_j} \frac{\partial P_l}{\partial x_m} \eta_s \eta_t. \quad (9)$$

Upon substituting  $\vec{\eta}_0 = \eta_0(\frac{1}{\sqrt{2}}, \frac{1}{\sqrt{2}}, 0)$ , these terms contribute to free energy as

$$\Delta F = \frac{1}{2} \eta_0^2 \sum_{i,j} \gamma_{ijlm} \frac{\partial P_i}{\partial x_i} \frac{\partial P_l}{\partial x_m}. \quad (10)$$

The symmetry of the  $\gamma_{ijlm}$  tensor is not cubic, as that of  $D_{ijlm}$ , but orthorhombic with the main axes along  $\vec{a}_{\text{IM}}$  ( $[-1\ 1\ 0]$ ),  $\vec{b}_{\text{IM}}$  ( $[1\ 1\ 0]$ ), and  $\vec{c}_{\text{IM}}$  ( $[0\ 0\ 1]$ ). The coefficient  $\gamma_{abab}$ , which determines the dispersion of transverse polarization waves propagating along  $\vec{b}_{\text{IM}}$  and polarized along  $\vec{a}_{\text{IM}}$  reads

$$\gamma_{abab} = \gamma_{xxyy} - \gamma_{yyyy} + \frac{1}{2}(\gamma_{xxxx} - \gamma_{xxyy} + \gamma_{xyxy} - \gamma_{xyyx}). \quad (11)$$

This coefficient is different from  $\gamma_{baba}$ , which corresponds to similar waves, but propagating along  $\vec{b}_{\text{IM}}$ . Therefore, biquadratic coupling between the polarization gradient and tilts can be sufficient for creating the incommensurate stiffness minima selectively at  $\vec{q}_0 = \pm(\xi, \xi, 0)$ , without simultaneously creating such minima at all the wave vectors of the same star.

The correlation energy for transverse waves propagating along  $\vec{b}_{\text{IM}}$  is defined by constant  $D_2$ , which is recalculated from tensors as

$$D_2 = (D_{xxxx} - D_{xxyy}) + \gamma_{abab} \eta_0^2. \quad (12)$$

For an incommensurate stiffness minimum this coefficient shall be less than zero.

### 4. Expected temperature dependencies of coefficients

Following the general philosophy of Landau-like models, such as Devonshire's [31], one tries to find a minimal number

of parameters that depend on temperature, ideally, one parameter, which is linear in  $T$ , as in Landau theory [34]. Here, one needs at least two parameters, because in the cubic phase both the ferroelectric and AFD modes appear soft and the model does not present a natural mechanism of linking one softening to the other. Therefore, the simplest model would be with both dielectric and AFD stiffness following linear trends,

$$\alpha(T) = A(T - T_0) \quad (13)$$

and

$$\alpha_{\text{AFD}}(T) = A_{\text{AFD}}(T - T_0^{\text{AFD}}). \quad (14)$$

Landau theory does not allow  $Pm\bar{3}m \rightarrow Imma$  AFD transition to be of second order [61]. On the other hand, the temperature dependence of  $R$ -point reflections appear linear in the IM phase (Fig. 2), which would be consistent with second-order transition. The simplest reconciliation is to assume that the transition is of “weakly” first order and  $\eta_0^2$  is not strictly, but *nearly* linear just below cubic  $\rightarrow$  IM transition,

$$\eta_0^2 \approx Y(T_0^{\text{AFD}} - T) \quad (15)$$

(above  $\approx T_0^{\text{AFD}}$ ,  $\eta_0^2 = 0$ ). The polarization correlation energy constant will then be also nearly linear [Eq. (12)] and decrease on cooling if  $\gamma_{abab}$  is negative. Figure 11 shows how  $q$ -dependent stiffness evolves in this case. Note that this behavior is ultimately simplified: along with the assumptions above, biquadratic coupling to homogeneous polarization (as opposed to the coupling to gradients) is neglected. The specifics of this minimal model is that the stiffness minimum shifts from zero in wave-vector space nearly continuously, similarly to how the free-energy minimum shifts from zero along the polarization axis in Landau theory of second-order transitions.

### C. Model vs experiment

This section examines the experimental data in comparison with the minimal model outlined above. There are no attempts to fit the data using model temperature dependencies (they are considerably different), but rather the  $q$ -dependent stiffness is modeled by the respective formula  $S(q) = \alpha_{\text{FE}} + D_2q^2 + D_4q^4$  [Figs. 12(a)–12(c)] at each temperature point and the resulting temperature dependencies of coefficients [Figs. 12(d) and 12(e)] are compared with expectations [Figs. 11(c) and 11(f)]. The fitting result with temperature-independent  $D_4$ , in our opinion, differs in shape with experiment in the high-temperature region of the cubic phase. So, we tried also a temperature-dependent  $D_4$ , which agrees better. The profiles in Figs. 12(a) and 12(b) correspond to  $T > 181^\circ\text{C}$ . The fits of these profiles appear reasonable. On the other hand, at lower temperatures ( $173^\circ\text{C} < T < 179^\circ\text{C}$ ) the fits appear inadequate, as Fig. 12(c) illustrates: the shape is clearly different.

Both  $\alpha$  and  $D_2$  decrease on cooling in the cubic and IM phases. This is especially remarkable for  $D_2$ : while it is expected to change in the IM phase due to interaction with tilts [Eq. (12) and Fig. 11(f)], in the cubic phase it is not expected to change. In Landau theory it is temperature independent [33], and one could expect this to extend qualitatively to Landau-like models. For the present crystal this seems to not apply, likely because it is not so similar to ferroelectrics; at

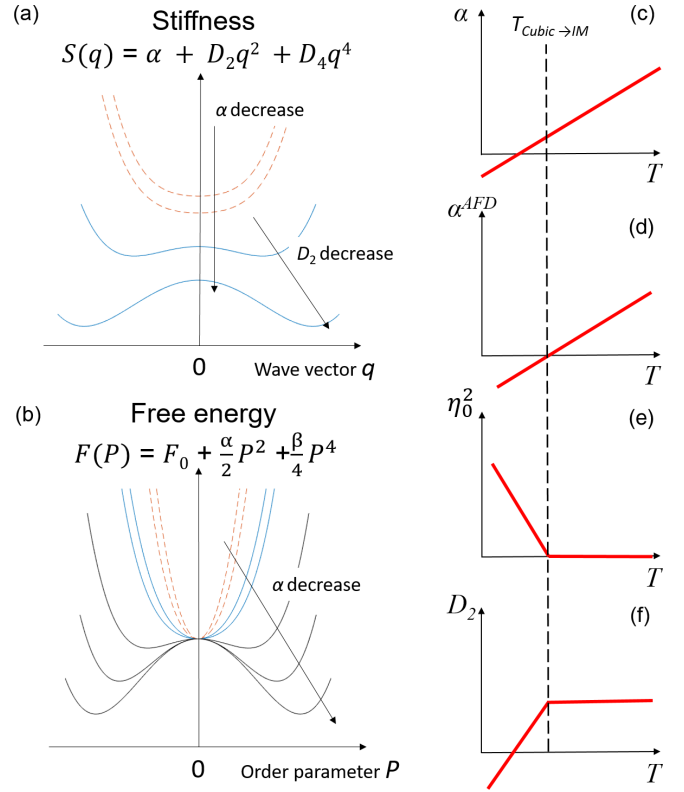


FIG. 11. Minimal Landau-like model of the IM phase in the temperature domain. Ferroelectric stiffness,  $\alpha$ , decreases linearly across the cubic  $\rightarrow$  IM transition. In the cubic phase (dashed red lines) this leads to homogeneous shift of the whole stiffness dispersion in (a) and to the unbending of the free-energy parabolic part in (b). In the IM phase (blue solid lines), the polarization correlation energy,  $D_2$ , linearly decreases due to the biquadratic interaction of the polarization gradient with oxygen octahedral tilts. This leads to the unbending of stiffness dispersion in (a) and the formation of incommensurate stiffness minimum. Subsets (c)–(f) describe the temperature behavior of the model parameters: dielectric stiffness  $\alpha$ , AFD stiffness  $\alpha_{\text{AFD}}$ , squared AFD order parameter  $\eta_0^2$ , and correlation energy constant  $D_2$ , respectively.

least its  $\alpha(T)$  does considerably violate  $\alpha = A(T - T_0)$  law and no ferroelectric phase forms.

Upon noting the interesting temperature dependence of  $D_2$  in the fits, it is instructive to attempt to ensure that this effect is real and not an artifact of the data processing. Figure 13 supports the fit results by showing stiffness profiles, recomputed so that the y axis becomes  $\sqrt{S - S_0}$ , where  $S$  is the stiffness and  $S_0$  is the stiffness at the zone center, as obtained by the fit. This way the parabolic stiffness curve is transformed to a linear curve with the slope of  $\sqrt{D_2}$ . This slope increases with temperature.

## V. DISCUSSION

### A. Relation to other observations of intermediate phase

The present IM phase is similar to the additional phase in pure  $\text{PbHfO}_3$  that is stabilized under pressure, where similar diffuse incommensurate maxima, as well as the  $R$ -point reflections, were also registered [46]. There are subtle

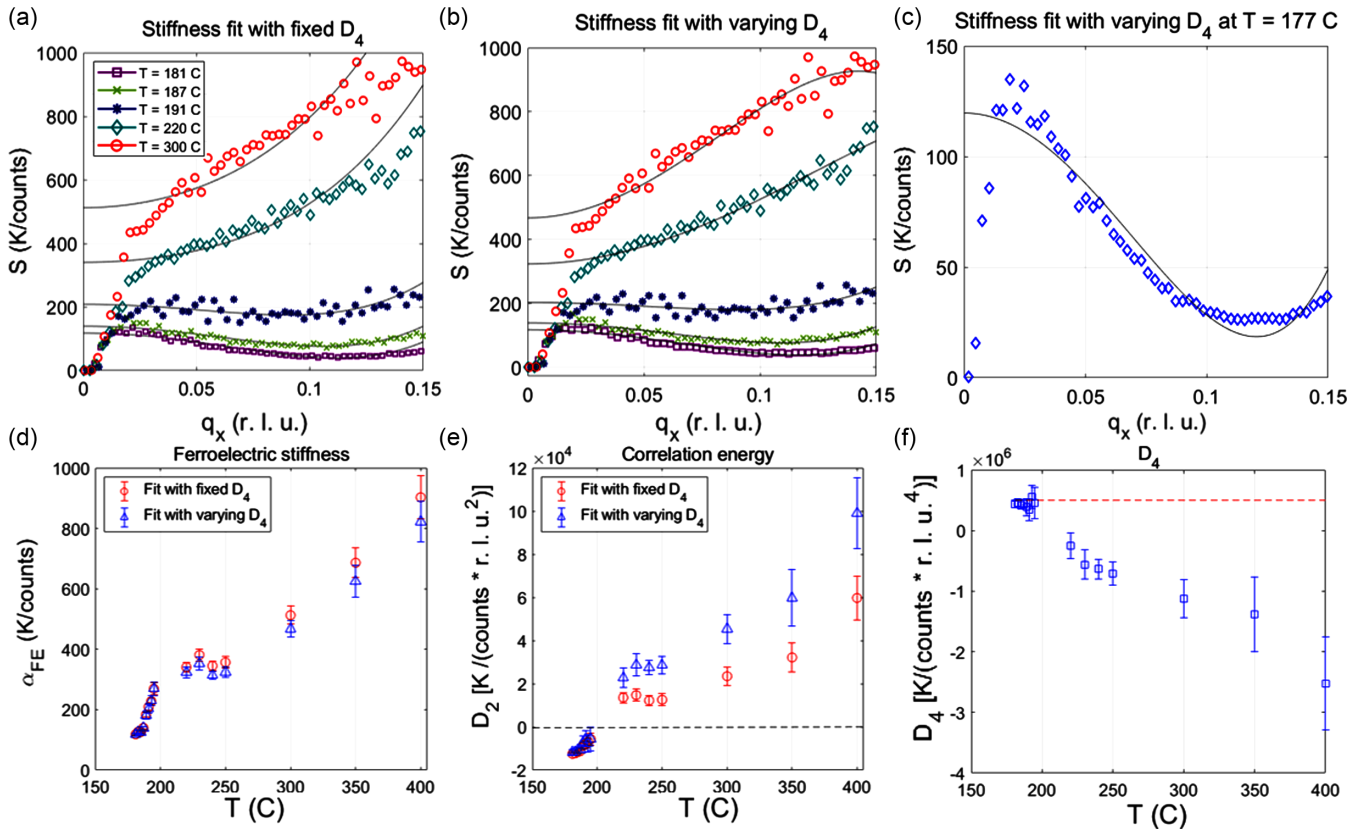


FIG. 12. Description of the stiffness profiles along the  $[1\ 1\ 0]$  direction by the relation  $S(q) = \alpha_{FE} + D_2 q^2 + D_4 q^4$ , where  $\alpha_{FE}$  is the ferroelectric stiffness and  $D_2$  is the polarization correlation energy constant. At low  $q_x$  values, the Bragg scattering and scattering by acoustic phonons are dominant, so stiffness fit is done for  $0.03 < q_x < 0.15$  reciprocal lattice units (r.l.u.). The  $\alpha_{FE}$  and  $D_2$  values are presented in non-SI units; to switch to SI units, it is necessary to multiply the absolute values of the parameters by  $N_1 = 1.23 \times 10^5$  [Jm/C<sup>2</sup>] (for the stiffness) and  $N_2 = 2.05 \times 10^{-14}$  [Jm<sup>3</sup>/C<sup>2</sup>] (for the  $D_2$ ), respectively. The stiffness in this figure is the same in meaning as in Fig. 7, but slightly differs in value due to different methods of obtaining it: Fig. 7 obtained from the fit of the intensity (proportional to the susceptibility) taking into account only  $D_2$ , and here it was done from the fit of the stiffness, taking into account also  $D_4$ .

differences, however, in part due to the presence of weak reflections at  $X$  and  $M$  points under pressure, which the IM phase in  $\text{PbHfO}_3\text{-PbSnO}_3$  lacks. Similar incommensu-

rate maxima were also seen in  $\text{PbZrO}_3$  under pressure [14], although, unfortunately, without information on the  $R$ -point superstructures. Most likely, all these phases are similar. Other studies of  $\text{PbHfO}_3\text{-PbSnO}_3$  [51,62], where  $\text{PbSnO}_3$  concentration was lower, did not reveal such a temperature-dependent incommensurate diffuse scattering maxima. Tentatively, this behavior changes strongly with tin concentration.

There is a disagreement between the temperature trend of the IM-phase dielectric stiffness obtained by diffraction [see Fig. 12(d)] and the corresponding trend obtained by dielectric measurements [48]. From diffraction, dielectric stiffness should decrease on cooling, while from dielectric measurements it should increase. We think this discrepancy comes likely from the polydomain structure of the IM phase. The agreement tends to recover (Fig. 14), if one considers a stiffness produced by averaging diffuse-scattering-derived values related to displacements along different  $\{110\}$  directions, which is more reminiscent to what is measured in a dielectric setup.

A research strategy applied to  $\text{Pb}(\text{Hf}_{0.7}\text{Sn}_{0.3})\text{O}_3$  in this work can also be introduced to a wider range of materials including lead-free ones. Primarily, one could look at bismuth-ferrite-based materials, in which incommensurate waves propagate in the same direction, but have much smaller

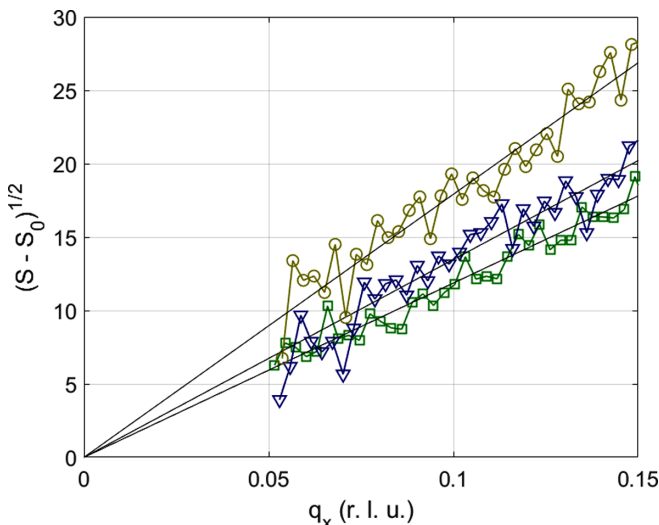


FIG. 13. The square root of the  $q$ -dependent part of the stiffness profiles along the  $[1\ 1\ 0]$  direction in the cubic phase. Slopes correspond to  $\sqrt{D_2}$ .

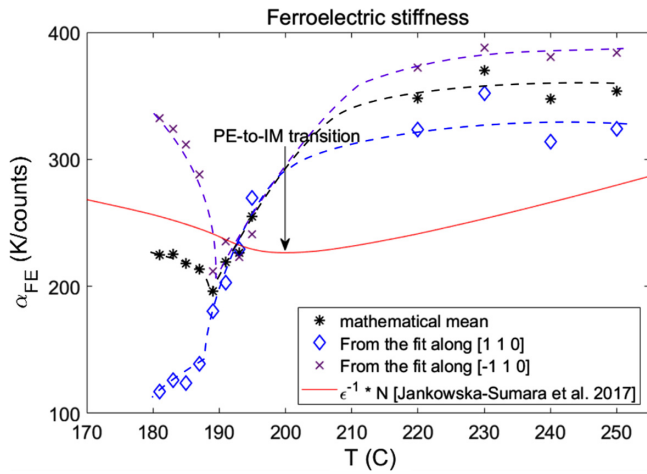


FIG. 14. Ferroelectric stiffness values extracted from diffuse scattering profiles along the  $[1\ 1\ 0]$  and  $[-1\ 1\ 0]$  directions. The average of those values is compared with the dielectric data of Jankowska-Sumara *et al.* [48]. One notes that averaging over two different directions results in better agreement in temperature trends below the transition point than the stand-alone values related to different directions.

period, while being also affected by octahedral tilts [63]. In other incommensurate materials, for example  $\text{NaNbO}_3$ -based [64], such an IM phase, if it exists, should be likely different because the incommensuration in these materials is related to other types of waves. Similar to  $\text{PbHfSnO}_3$ , diffuse scattering landscapes can be observed in  $\text{Pb}_2\text{ScTaO}_6$  [65], which allows one to expect a similar physical background in Pb-containing relaxors.

### B. Effect of Sn doping on structural distortions

The influence of Sn doping on different types of distortions can be most straightforwardly grasped from a phase diagram in temperature-doping coordinates, as published in [62]. Sn doping increases the temperature, at which the cubic phase transforms to the IM phase. It can be deduced that Sn doping increases the stability of antiphase tilts. On the other hand, Sn doping decreases the temperature, at which the IM phase transforms to the IC phase. Therefore, the stability of IC ordering is suppressed by Sn doping. What remains not covered by such a phase diagram is the interaction of Sn doping with ferroelectric order parameter. To this end, it is possible to learn from the fact that Sn doping increases the coercive field in  $\text{PbHfO}_3$  ceramics [66], which can be interpreted as destabilizing the (metastable) ferroelectric phase even more intensively than it destabilizes the incommensurate phase. This property of Sn, as observed upon doping  $\text{PbHfO}_3$ , is qualitatively consistent with the observations in  $\text{BaTiO}_3$  [67,68], where Sn also destabilizes the ferroelectric order, but this time in favor of polar nanoregions.

### C. Inhomogeneous polarization is not sufficient for modeling incommensurate fluctuations in the lower- $T$ part of the IM phase

It is remarkable that the minimal symmetry-based Landau-like model describes the data not so well, as the comparison

of Figs. 11 and 12 highlights. The discrepancies between model and experiment [Fig. 12(c)] arise surprisingly quickly, at about  $20^\circ\text{C}$  below the cubic  $\rightarrow$  IM transition. Normally, one should expect the validity region for Landau-like models of ferroelectrics to be larger, which is related to the experimental temperatures being small when compared to the so-called “atomic temperature” of about  $10^4$ – $10^5$  K [34]. Therefore, the origin of these discrepancies is presently unclear.

What one may suggest from the discrepancy of Fig. 12(c) is that the incommensurate order parameter, when its wave vector is considerably away from the zone center, cannot be interpreted as just an inhomogeneous polarization. It is not necessary due to stiffness renormalization by flexoelectric or similar interactions, but may be simply because sufficiently away from the zone center the waves cannot be considered as weakly inhomogeneous. An independent order parameter should be introduced instead, for which the symmetry-allowed expansion around its wave vector,  $\vec{q}_0$ , is expected to be adequate in the vicinity of IM  $\rightarrow$  incommensurate transition. An experimental indication towards this is the linear dependence of incommensurate stiffness near that transition [Fig. 9(b)], which is compatible with classical models of incommensurate transitions with explicitly defined incommensurate order parameter [36]. If, instead, one assumes that incommensurate stiffness follows ferroelectric softening, as in the minimal model considered here, the incommensurate stiffness would be quadratic in temperature, which contradicts the observations. It seems appropriate to suggest that the dielectric stiffness may not be a very successful candidate for being a critical parameter in models like this, despite the experimental increase of  $\epsilon(T)$  on cooling in the cubic phase.

### D. Minimal model with gradient terms as a generalization of Holakovskiy’s model of triggered ferroelectricity

The relation of dipole ordering to the tilts subsystem in perovskite and similar structures is widely discussed [3,12,18,22–24,30,44,60,69–71]. The likely initial point of that discussion is Holakovskiy’s proposition [60] on a possibility that it is the octahedral tilt subsystem that can be a “soft” instead of a “ferroelectric” subsystem, while the ferroelectric transition still takes place due to a positive biquadratic interaction between those. The present paper attempts to extend this to inhomogeneous polarization by considering biquadratic coupling also to polarization gradients. This appears successful in the higher- $T$  region of the IM phase, where incommensurate fluctuations occur near the zone center, but fails at the low- $T$  region, where the fluctuations are of much shorter wavelength [ $q \approx (1/7, 1/7, 0)$ ]. In pure  $\text{PbHfO}_3$ , the region of an apparent validity of the minimal model is skipped, because the IM phase itself is skipped, and the incommensurate modulations are of relatively short wavelength from the very beginning. The minimal model is, therefore, unlikely sufficient (although it is conceptually consistent) for describing a triggered incommensurate transition in pure  $\text{PbHfO}_3$  [44] and a more complicated model is needed.

### E. A possibility of temperature-independent characteristic length scale for inhomogeneities

Polarization correlation energy constant,  $D_2$ , appears to follow a similar temperature trend to that of ferroelectric stiffness: they both decrease nearly linearly in the cubic phase with a critical temperature of about 200 °C. If one composes the correlation length parameter from those as  $\sqrt{D_2/\alpha}$ , this parameter appears rather temperature independent. If so, one should think that this length scale is characteristic to the system in a wide temperature range. Upon estimating this length scale from Figs. 12(d) and 12(e), one arrives at the value of about ten lattice units (projected to pseudocubic high-symmetry directions). This value is comparable to the period of incommensurate phase, which is  $\approx 7$  lattice units. A natural suggestion seems to be that the fluctuations of polarization, even in the cubic phase, are on average as inhomogeneous as the incommensurate phase is, although the level of order differs drastically, from long-range order in the incommensurate phase through short-range correlated incommensurate fluctuations in the IM phase and to, apparently, much more disordered fluctuations in the cubic phase. This is similar to how the local structure of some perovskites appears largely temperature independent despite drastic changes in the macroscopic symmetry and structure [72,73].

## VI. CONCLUSION

The x-ray diffuse scattering experiment has shown a rich spectrum of unusual behavior associated with phase transitions in Sn-doped  $\text{PbHfO}_3$ . Among the most important takeaways is a crossover from ferroelectric fluctuations in the cubic phase to incommensurate fluctuations in the IM phase. It appears convincing that this crossover occurs mainly due to the interaction with octahedral tilts, which are the IM phase order parameter. Quantifying this behavior within a model turns out to be complicated; few conceptual challenges emerge. The ferroelectric stiffness deviates from Curie-Weiss law already in the cubic phase, and it is not clear how a Landau-like model should account for this. Trying to keep the discussion within the realm of Landau-like models, one may try connecting the stiffness saturation with some “background stiffness,” the phenomenological quantity to be introduced in analogy with the “background permittivity” of Tagantsev and co-workers [74]. We hope that the discrepancies in describing

the phase transitions in lead-based antiferroelectrics within Landau-like models will be resolved in the near future upon advancing in the experimental characterization of this and similar systems, and also possibly by drawing from related fields such as relaxor ferroelectrics.

## ACKNOWLEDGMENTS

N. Ter-Oganessian and Peng Chen are acknowledged for useful discussions on symmetry-related subjects. M. Polentarutti and G. Bais are acknowledged for useful discussions and proofreading. A. Bosak is acknowledged for his help with experiment and useful discussions. The reported study was supported by Russian Foundation for Basic Research, Projects No. 20-32-90176 and No. 20-32-70215. The authors acknowledge the European Synchrotron Radiation Facility for the provision of synchrotron radiation facilities. M.P. was supported by Operational Program Research, Development and Education (financed by European Structural and Investment Funds and by the Czech Ministry of Education, Youth, and Sports), Project No. SOLID21-CZ.02.1.01/0.0/0.0/16\_019/0000760.

## APPENDIX

### 1. Structure factor for diffuse scattering by a simple lattice

In the approximation of small displacements,  $\vec{U}_i$ , from high-symmetry positions,  $\vec{R}_i$ , the total structure factor for a simple lattice can be expanded as follows (the Debye-Waller factor and normalization factors are omitted for simplicity).

$$\begin{aligned} F(\vec{Q}) &= f(\vec{Q}) \sum_i \exp(i\vec{Q}\vec{r}_i) = f(\vec{Q}) \sum_i \exp[i\vec{Q}(\vec{R}_i + \vec{U}_i)] \\ &\approx f(\vec{Q}) \sum_i \exp(i\vec{Q}\vec{R}_i)(1 + i\vec{Q}\vec{U}_i) \\ &= f(\vec{Q})\delta(\vec{Q} - \vec{\tau}) + if(\vec{Q})(\vec{Q}\vec{U}_q)\delta(\vec{Q} - \vec{q} - \vec{\tau}), \quad (\text{A1}) \end{aligned}$$

where  $f(\vec{Q})$  is the atomic scattering factor and  $\vec{U}_q$  is the Fourier component of displacements. In the last row, the former term corresponds to a contribution of this sublattice to the Bragg scattering structure factor, and the latter to the structure factor for diffuse scattering.

[1] C. Kittel, Theory of antiferroelectric crystals, *Phys. Rev.* **82**, 729 (1951).  
 [2] W. Lawless, Ferroelectricity and antiferroelectricity in  $\text{BaTiO}_3$ , *J. Phys. Soc. Jpn.* **23**, 325 (1967).  
 [3] L. Bellaiche and J. Íñiguez, Universal collaborative couplings between oxygen-octahedral rotations and antiferroelectric distortions in perovskites, *Phys. Rev. B* **88**, 014104 (2013).  
 [4] K. M. Rabe, Antiferroelectricity in oxides: A reexamination, *Functional Metal Oxides: New Science and Novel Applications*, edited by S. B. Ogale, T. V. Venkatesan, and M. G. Blamire (Wiley-VCH Verlag GmbH & Co. KGaA, Weinheim, Germany, 2013), pp. 221–244.

[5] X. Wei, A. Tagantsev, A. Kvasov, K. Roleder, C. Jia, and N. Setter, Ferroelectric translational antiphase boundaries in non-polar materials, *Nat. Commun.* **5**, 3031 (2014).  
 [6] M. Pesic, S. Knebel, M. Hoffmann, C. Richter, T. Mikolajick, and U. Schroeder, How to make DRAM non-volatile? Antiferroelectrics: A new paradigm for universal memories, in *2016 IEEE International Electron Devices Meeting (IEDM)* (IEEE, New York, 2016), pp. 11.6.1–11.6.4.  
 [7] M. Park and C. Hwang, *Ferroelectric-Gate Field Effect Transistor Memories* (Springer, New York, 2016), p. 295.  
 [8] B. Xu, J. Íñiguez, and L. Bellaiche, Designing lead-free antiferroelectrics for energy storage, *Nat. Commun.* **8**, 15682 (2017).

- [9] C. A. Randall, Z. Fan, I. Reaney, L.-Q. Chen, and S. Trolier-McKinstry, Antiferroelectrics: History, fundamentals, crystal chemistry, crystal structures, size effects, and applications, *J. Am. Ceram. Soc.* **104**, 3775 (2021).
- [10] D. Viehland, D. Forst, and J.-F. Li, Compositional heterogeneity and the origins of the multicell cubic state in Sn-doped lead zirconate titanate ceramics, *J. Appl. Phys.* **75**, 4137 (1994).
- [11] Y. Cai, F. Phillipp, A. Zimmermann, L. Zhou, F. Aldinger, and M. Rühle, TEM study of superstructure in a perovskite lead lanthanum zirconate stannate titanate ceramic, *Acta Mater.* **51**, 6429 (2003).
- [12] A. Tagantsev, K. Vaideswaran, S. Vakhruhev, A. Filimonov, R. Burkovsky, A. Shaganov, D. Andronikova, A. Rudskoy, A. Baron, H. Uchiyama *et al.*, The origin of antiferroelectricity in PbZrO<sub>3</sub>, *Nat. Commun.* **4**, 2229 (2013).
- [13] N. Zhang, M. Paściak, A. Glazer, J. Hlinka, M. Gutmann, H. A. Sparkes, T. Welberry, A. Majchrowski, K. Roleder, Y. Xie *et al.*, A neutron diffuse scattering study of PbZrO<sub>3</sub> and Zr-rich PbZr<sub>(1-x)</sub>Ti<sub>x</sub>O<sub>3</sub>, *J. Appl. Crystallogr.* **48**, 1637 (2015).
- [14] R. Burkovsky, I. Bronwald, D. Andronikova, B. Wehinger, M. Krisch, J. Jacobs, D. Gambetti, K. Roleder, A. Majchrowski, A. Filimonov *et al.*, Critical scattering and incommensurate phase transition in antiferroelectric PbZrO<sub>3</sub> under pressure, *Sci. Rep.* **7**, 41512 (2017).
- [15] A. Bosak, V. Svitlyk, A. Arakcheeva, R. Burkovsky, V. Diadkin, K. Roleder, and D. Chernyshov, Incommensurate crystal structure of PbHfO<sub>3</sub>, *Acta Crystallogr., Sect. B: Struct. Sci., Cryst. Eng. Mater.* **76**, 7 (2020).
- [16] M. J. Haun, T. Harvin, M. T. Lanagan, Z. Zhuang, S. Jang, and L. Cross, Thermodynamic theory of PbZrO<sub>3</sub>, *J. Appl. Phys.* **65**, 3173 (1989).
- [17] A. Bussmann-Holder, J.-H. Ko, A. Majchrowski, M. Górný, and K. Roleder, Precursor dynamics, incipient ferroelectricity and huge anharmonicity in antiferroelectric lead zirconate PbZrO<sub>3</sub>, *J. Phys.: Condens. Matter* **25**, 212202 (2013).
- [18] J. Íñiguez, M. Stengel, S. Prosandeev, and L. Bellaiche, First-principles study of the multimode antiferroelectric transition in PbZrO<sub>3</sub>, *Phys. Rev. B* **90**, 220103(R) (2014).
- [19] J. Hlinka, T. Ostapchuk, E. Buixaderas, C. Kadlec, P. Kuzel, I. Gregora, J. Kroupa, M. Savinov, A. Klic, J. Drahokoupil *et al.*, Multiple Soft-Mode Vibrations of Lead Zirconate, *Phys. Rev. Lett.* **112**, 197601 (2014).
- [20] K. Patel, S. Prosandeev, Y. Yang, B. Xu, J. Íñiguez, and L. Bellaiche, Atomistic mechanism leading to complex antiferroelectric and incommensurate perovskites, *Phys. Rev. B* **94**, 054107 (2016).
- [21] P. Tolédano and M. Guennou, Theory of antiferroelectric phase transitions, *Phys. Rev. B* **94**, 014107 (2016).
- [22] R. G. Burkovsky, Dipole-dipole interactions and incommensurate order in perovskite structures, *Phys. Rev. B* **97**, 184109 (2018).
- [23] B. Xu, O. Hellman, and L. Bellaiche, Order-disorder transition in the prototypical antiferroelectric PbZrO<sub>3</sub>, *Phys. Rev. B* **100**, 020102(R) (2019).
- [24] W. Schranz, A. Tröster, and I. Rychetsky, Contributions to polarization and polarization switching in antiphase boundaries of SrTiO<sub>3</sub> and PbZrO<sub>3</sub>, *J. Appl. Phys.* **128**, 194101 (2020).
- [25] R. W. Whatmore and A. M. Glazer, Structural phase transitions in lead zirconate, *J. Phys. C: Solid State Phys.* **12**, 1505 (1979).
- [26] D. Singh, Structure and energetics of antiferroelectric PbZrO<sub>3</sub>, *Phys. Rev. B* **52**, 12559 (1995).
- [27] U. Waghmare and K. Rabe, Lattice instabilities, anharmonicity and phase transitions in PbZrO<sub>3</sub> from first principles, *Ferroelectrics* **194**, 135 (1997), Fourth Williamsburg Workshop On First-Principles Calculations for Ferroelectrics, 1996.
- [28] P. Ghosez, E. Cockayne, U. V. Waghmare, and K. M. Rabe, Lattice dynamics of BaTiO<sub>3</sub>, PbTiO<sub>3</sub>, and PbZrO<sub>3</sub>: A comparative first-principles study, *Phys. Rev. B* **60**, 836 (1999).
- [29] M. Paściak, T. Welberry, A. Heerdegen, V. Laguta, T. Ostapchuk, S. Leoni, and J. Hlinka, Atomistic modeling of diffuse scattering in cubic PbZrO<sub>3</sub>, *Phase Transitions* **88**, 273 (2015).
- [30] B. K. Mani, S. Lisenkov, and I. Ponomareva, Finite-temperature properties of antiferroelectric PbZrO<sub>3</sub> from atomistic simulations, *Phys. Rev. B* **91**, 134112 (2015).
- [31] A. Devonshire, XCVI. Theory of barium titanate, *London, Edinburgh, Dublin Philos. Mag. J. Sci.* **40**, 1040 (1949).
- [32] P. Marton and J. Hlinka, Simulation of domain patterns in BaTiO<sub>3</sub>, *Phase Transitions* **79**, 467 (2006).
- [33] L. Landau and E. Lifshitz, *Statistical Physics* (Elsevier Science, New York, 2013), Vol. 5.
- [34] A. P. Levanyuk, I. B. Misirlioglu, and M. B. Okatan, Landau, Ginzburg, Devonshire and others, *Ferroelectrics* **569**, 310 (2020).
- [35] P. Tolédano and D. D. Khalyavin, Symmetry-determined antiferroelectricity in PbZrO<sub>3</sub>, NaNbO<sub>3</sub>, and PbHfO<sub>3</sub>, *Phys. Rev. B* **99**, 024105 (2019).
- [36] R. Blinc and A. Levanyk, *Incommensurate Phases in Dielectrics* (North-Holland, Amsterdam, 1986).
- [37] V. Heine and J. McConnell, The origin of incommensurate structures in insulators, *J. Phys. C* **17**, 1199 (1984).
- [38] P. Saint-Gregoire, Role of the coupling between strains and order parameter gradient in crystals, *Phase Transitions* **67**, 587 (1999).
- [39] M. Stengel, Unified *ab initio* formulation of flexoelectricity and strain-gradient elasticity, *Phys. Rev. B* **93**, 245107 (2016).
- [40] J. Axe, J. Harada, and G. Shirane, Anomalous acoustic dispersion in centrosymmetric crystals with soft optic phonons, *Phys. Rev. B* **1**, 1227 (1970).
- [41] E. Farhi, A. Tagantsev, R. Currat, B. Hehlen, E. Courtens, and L. Boatner, Low energy phonon spectrum and its parameterization in pure KTaO<sub>3</sub> below 80 K, *Eur. Phys. J. B* **15**, 615 (2000).
- [42] A. Bussmann-Holder, K. Roleder, and J.-H. Ko, Instabilities in the ferro- and antiferroelectric lead perovskites driven by transition metal ion mass: From PbTiO<sub>3</sub> via PbZrO<sub>3</sub> to PbHfO<sub>3</sub>, *J. Phys.: Condens. Matter* **26**, 275402 (2014).
- [43] D. Andronikova, Y. Bronwald, R. Burkovsky, D. Chernyshev, A. Filimonov, B. Nacke, Y. Zuo-Guang, and S. Vakhruhev, Critical X-ray scattering in mixed piezoelectric material PbZr<sub>0.6</sub>Ti<sub>0.4</sub>O<sub>3</sub>, *Solid State Phenom.* **245**, 211 (2016).
- [44] R. G. Burkovsky, I. Bronwald, D. Andronikova, G. Lityagin, J. Piecha, S.-M. Souliou, A. Majchrowski, A. Filimonov, A. Rudskoy, K. Roleder *et al.*, Triggered incommensurate transition in PbHfO<sub>3</sub>, *Phys. Rev. B* **100**, 014107 (2019).
- [45] G. Samara, Pressure and temperature dependence of the dielectric properties and phase transitions of the antiferroelectric perovskites: PbZrO<sub>3</sub> and PbHfO<sub>3</sub>, *Phys. Rev. B* **1**, 3777 (1970).
- [46] M. A. Knyazeva, D. Andronikova, G. Lityagin, I. A. Bronwald, P. Paraskevas, A. Majchrowski, K. Roleder, A. Filimonov, and

- R. Burkovsky, Phase transitions in lead hafnate under high pressure, *Phys. Solid State* **61**, 1759 (2019).
- [47] B. Jaffe, W. J. Cook, and J. Jaffe, *Piezoelectric Ceramics* (Academic Press, London, 1971).
- [48] I. Jankowska-Sumara, J.-H. Ko, M. Podgórna, S. H. Oh, and A. Majchrowski, Micro-Raman scattering and dielectric investigations of phase transitions behavior in the  $\text{PbHf}_{0.7}\text{Sn}_{0.3}\text{O}_3$  single crystal, *J. Appl. Phys.* **122**, 104104 (2017).
- [49] D. Corker, A. Glazer, W. Kaminsky, R. Whatmore, J. Dec, and K. Roleder, Investigation into the crystal structure of the perovskite lead hafnate,  $\text{PbHfO}_3$ , *Acta Crystallogr., Sect. B: Struct. Sci.* **54**, 18 (1998).
- [50] H. Fujishita, K. Kato, E. Nishibori, M. Takata, M. Sakata, and S. Katano, Structural modulations in the intermediate phase of antiferroelectric  $\text{PbHfO}_3$ , *J. Phys. Soc. Jpn.* **87**, 124603 (2018).
- [51] I. Jankowska-Sumara, M. Paściak, M. Kądziołka-Gaweł, M. Podgórna, A. Majchrowski, and K. Roleder, Local properties and phase transitions in Sn doped antiferroelectric  $\text{PbHfO}_3$  single crystal, *J. Phys.: Condens. Matter* **32**, 435402 (2020).
- [52] A. D. Bruce and R. A. Cowley, *Structural Phase Transitions* (Taylor & Francis, London, 1981).
- [53] B. Dorner, *Coherent Inelastic Neutron Scattering in Lattice Dynamics* (Springer-Verlag, Berlin, 1982).
- [54] A. Glazer, Simple ways of determining perovskite structures, *Acta Crystallogr., Sect. A: Cryst. Phys., Diffr., Theor. Gen. Crystallogr.* **31**, 756 (1975).
- [55] J. Axe and G. Shirane, Inelastic-neutron-scattering study of acoustic phonons in  $\text{Nb}_3\text{Sn}$ , *Phys. Rev. B* **8**, 1965 (1973).
- [56] R. Cowley and G. Shirane, On quasi-elastic scattering and surfaces in  $\text{SrTiO}_3$ , *J. Phys. C* **11**, L939 (1978).
- [57] P. V. Yudin, R. Ahluwalia, and A. K. Tagantsev, Upper bounds for flexoelectric coefficients in ferroelectrics, *Appl. Phys. Lett.* **104**, 082913 (2014).
- [58] See Supplemental Material at <http://link.aps.org/supplemental/10.1103/PhysRevB.105.014101> for ISOTROPY software output describing the symmetry-allowed terms of free-energy expansion in terms of polarization and tilts.
- [59] H. T. Stokes, D. M. Hatch, and B. J. Campbell, ISOTROPY software suite, <https://iso.byu.edu/iso/isowww.php>.
- [60] J. Holakovsky, A new type of the ferroelectric phase transition, *Physica Status Solidi B* **56**, 615 (1973).
- [61] C. J. Howard and H. T. Stokes, Group-theoretical analysis of octahedral tilting in perovskites, *Acta Crystallogr., Sect. B: Struct. Sci.* **54**, 782 (1998).
- [62] I. Jankowska-Sumara, J.-H. Ko, and A. Majchrowski, The complexity of structural phase transitions in  $\text{Pb}(\text{Hf}_{0.92}\text{Sn}_{0.08})\text{O}_3$  single crystals, *J. Am. Ceram. Soc.* **104**, 5990 (2021).
- [63] D. D. Khalyavin, A. N. Salak, A. B. Lopes, N. M. Olekhnovich, A. V. Pushkarev, Y. V. Radyush, E. L. Fertman, V. A. Desnenko, A. V. Fedorchenko, P. Manuel *et al.*, Magnetic structure of an incommensurate phase of La-doped  $\text{BiFe}_{0.5}\text{Sc}_{0.5}\text{O}_3$ : Role of antisymmetric exchange interactions, *Phys. Rev. B* **92**, 224428 (2015).
- [64] H. Guo, H. Shimizu, and C. A. Randall, Direct evidence of an incommensurate phase in  $\text{NaNbO}_3$  and its implication in  $\text{NaNbO}_3$ -based lead-free antiferroelectrics, *Appl. Phys. Lett.* **107**, 112904 (2015).
- [65] K. Baba-Kishi and M. Pasciak, An electron diffraction and Monte Carlo simulation study of an incommensurate antiferroelectric state in the relaxor ferroelectric  $\text{Pb}_2\text{ScTaO}_6$ , *J. Appl. Crystallogr.* **43**, 140 (2010).
- [66] P.-Z. Ge, X.-G. Tang, K. Meng, X.-X. Huang, S.-F. Li, Q.-X. Liu, and Y.-P. Jiang, Energy storage density and charge-discharge properties of  $\text{PbHf}_{1-x}\text{Sn}_x\text{O}_3$  antiferroelectric ceramics, *Chem. Eng. J.* **429**, 132540 (2022).
- [67] C. Lei, A. A. Bokov, and Z.-G. Ye, Ferroelectric to relaxor crossover and dielectric phase diagram in the  $\text{BaTiO}_3$ - $\text{BaSnO}_3$  system, *J. Appl. Phys.* **101**, 084105 (2007).
- [68] W. Xiaoyong, F. Yujun, and Y. Xi, Dielectric relaxation behavior in barium stannate titanate ferroelectric ceramics with diffused phase transition, *Appl. Phys. Lett.* **83**, 2031 (2003).
- [69] W. Zhong and D. Vanderbilt, Competing Structural Instabilities in Cubic Perovskites, *Phys. Rev. Lett.* **74**, 2587 (1995).
- [70] N. A. Benedek and C. J. Fennie, Hybrid Improper Ferroelectricity: A Mechanism for Controllable Polarization-Magnetization Coupling, *Phys. Rev. Lett.* **106**, 107204 (2011).
- [71] T. Gu, T. Scarbrough, Y. Yang, J. Íñiguez, L. Bellaiche, and H. J. Xiang, Cooperative Couplings between Octahedral Rotations and Ferroelectricity in Perovskites and Related Materials, *Phys. Rev. Lett.* **120**, 197602 (2018).
- [72] S. Teslic and T. Egami, Atomic structure of  $\text{PbZrO}_3$  determined by pulsed neutron diffraction, *Acta Crystallogr., Sect. B: Struct. Sci.* **54**, 750 (1998).
- [73] L. Jiang, D. C. Mitchell, W. Dmowski, and T. Egami, Local structure of  $\text{NaNbO}_3$ : A neutron scattering study, *Phys. Rev. B* **88**, 014105 (2013).
- [74] V. O. Sherman, A. K. Tagantsev, N. Setter, D. Iddles, and T. Price, Ferroelectric-dielectric tunable composites, *J. Appl. Phys.* **99**, 074104 (2006).